

Ring-o-rings: a new category of supramolecular structures with topologically tunable properties

L. Tubiana*

*Physics Department, University of Trento, via Sommarive, 14 I-38123 Trento, Italy
INFN-TIFPA, Trento Institute for Fundamental Physics and Applications, I-38123 Trento, Italy and
Faculty of Physics, University of Vienna, Boltzmannngasse 5, 1090 Vienna, Austria*

F. Ferrari

CASA and Institute of Physics, University of Szczecin, Wielkopolska 15, 70-451 Szczecin, Poland*

E. Orlandini

*Department of Physics and Astronomy, University of Padova, Via Marzolo 8, I-35131 Padova, Italy and
INFN, Sezione di Padova, Via Marzolo 8, I-35131 Padova, Italy*

(Dated: December 17, 2021)

Macrochains of topologically interlocked rings with unique physical properties have recently gained considerable interest in supramolecular chemistry, biology, and soft matter. Most of the work has been, so far, focused on linear chains and on their variety of conformational properties compared to standard polymers. Here we go beyond the linear case and show that, by circularizing such macrochains, one can exploit the topology of the local interlockings to store torsional stress in the system, altering significantly its metric and local properties. Moreover, by properly defining the twist (T_w) and writhe (W_r) of these macrorings we show the validity of a relation equivalent to the Călugăreanu-White-Fuller theorem $T_w + W_r = \text{const}$, originally proved for ribbon like structures such as ds-DNA. Our results suggest that circular structures of topologically linked rings with storable and tunable torsion can form a new category of highly designable multiscale structures with potential applications in supramolecular chemistry and material science.

Keywords: macromolecules, topology, coarse-graining, smart materials

Topologically constrained molecules and polymers have recently attracted considerable attention in physics, chemistry and biology [1]. Examples are nano-engineered Mechanically Interlocked Molecules (MIMs) such as rotaxanes, catenanes, and molecular knots [2, 3], melts of rings [4], and olympic gels [5–7] such as the natural occurring kinetoplast DNA [8–11]. Steady advancements in chemical synthesis techniques [12–14], modelling, and simulations [15, 16] have recently started to offer a framework to design systems of interlocked rings with controllable properties [13, 14, 17, 18] and versatile applications [19–21]. Examples range from catalyzers and nanomachines [22–26] to candidates for novel smart materials and artificial muscles [27].

Novel experimental techniques are now opening the possibility to synthesize high-weight polycatenanes, called Mechanically Interlocked Polymers (MIPs), long chains composed by n elementary rings held together only by topological interlocking [13, 14, 28]. In particular, in [13] metal supramolecular polymers were used to obtain polycatenanes composed of up to $n = 130$ rings, while in [14] a novel self-assembly technique was proposed in which supramolecular rings were grown directly to form a catenane of up to 22 units [14]. These studies have prompted the question of how the configurational properties of MIPs differ from their standard polymeric counterparts whose elementary units are held together by covalent bonds [29–32].

Interestingly, in [13] it was also demonstrated the possibility to synthesize cyclic polycatenanes. This brings up the question on how and to which extent the imposed circular constraint can affect the physical properties of these supramolecular structures. For instance, circularized polycatenanes may assume supercoiled configurations as in dsDNA, significantly affecting their elastic and dynamical properties, and, arguably, their responsiveness to external stimuli.

Here we show that circular polycatenanes can store supramolecular torsion upon circularization and, by using extensive molecular dynamics simulations, we characterize their equilibrium properties as a function of the number of elementary rings n and the amount of supramolecular torsion trapped into the system. Our results show that this controls the average extension of the macrochains as well as their local properties such as the relative orientation of the rings. Finally, by extending to the present case the notion of twist and writhe used in ribbon-like structures such as the ds-DNAs, we show that a relation equivalent to the Călugăreanu-White-Fuller theorem holds also for circular polycatenanes.

Our reference system consists of n semiflexible oriented rings (the elementary units of the polycatenane) each composed of $m = 48$ beads with nominal diameter σ . This level of polymerization has been chosen to obtain elementary rings with a thickness to diameter ratio, $p = \frac{\sigma}{D}$, similar to the one typically achieved in polycate-

nanos obtained from metal-supramolecular polymers [13]. Other values of p , compatible with DNA minicircles [3] and supramolecular toroids [14] have been investigated too. The connectivity of each elementary ring is provided by a FENE potential while the ring's nominal persistence length is set to $l_p = 2m\sigma$, preventing substantial variations in its local curvature due to thermal fluctuations (see Fig. 1a). This level of rigidity is compatible with those of the rings used both in [13] and [14]. The excluded-volume interaction among the nm beads is treated via a Weeks-Chandler-Andersen (WCA) potential, see SM.

We consider closed polycatenanes formed by $n = 2k$ rings, connected in such a way that they can always be arranged into a planar circle. Adopting this configuration as a reference, we orient the rings so that all their normals point either above or below the plane. Specifically, for each ring i we define its normal as $\mathbf{N}_i = \frac{4}{m} \sum_{k=1}^{m/4} (\mathbf{r}_{k+m/4} - \mathbf{R}_i) \times (\mathbf{r}_k - \mathbf{R}_i)$, where \mathbf{r}_k is the position of the k -th bead on ring i , oriented as above, \mathbf{R}_i is its center of mass, and $\hat{\mathbf{N}}_i = \mathbf{N}_i/|\mathbf{N}_i|$. We then assign a linking number $Lk_{i,i+1}$, to all pair of rings $i, i+1$ (with $n+1=1$) according to the standard convention for the sign of crossings, see Fig. 1. In this way one can distinguish three classes of rings forming the circular polycatenanes: 0-rings, which form a +1 and a -1 Hopf link with their neighbours (in blue in Fig. 1), and +2(-2) rings, which contribute two +1(-1) Hopf links (in red and yellow respectively in Fig. 1c, d)). Clearly, the linking numbers of all ring pairs can be univocally identified by fixing the type of either even- or odd-numbered rings. Furthermore, in the planar conformation, 0-rings can rotate around the axis identified by the centers of their neighbours along the chain by an angle $\phi(p)$ without affecting their neighbours, while the same is not possible for +2 and -2 rings. Thus, the latter can be thought to induce a torsion in the polycatenane.

Using the setting above, we identify the supramolecular torsion captured by circularization with $n_{tr} = n_+ - n_-$ where n_+ and n_- are the number of +2 (red) -2 rings (yellow) respectively. Clearly, $n_{tr} = \frac{1}{2} \sum_{i=1}^n Lk_{i,i+1}$, where $Lk_{i,i+1} \in \{-1, +1\}$ is the linking number of the pair of rings $(i, i+1)$, with $n+1=1$. Given the constraint that all polycatenanes must admit a planar conformation as in Fig. 1 c), n_{tr} can only take values between $-n/2$ and $n/2$.

We note that for circular polycatenanes n_{tr} is conserved, while the number and position of 0, +2 and -2 rings can vary. This can be easily seen by rotating the gray ring marked 1 in Fig. 1c) and then reorienting the rings so that their normals point up. The resulting catenane, shown in Fig. 1d), still has the same value of n_{tr} , no matter whether we count it on the odd or even rings. As shown in the SM, all different labelings of the rings giving a fixed value of n_{tr} can be mapped to a reference

polycatenane having n_{tr} +2-rings and $n/2 - n_{tr}$ 0-rings.

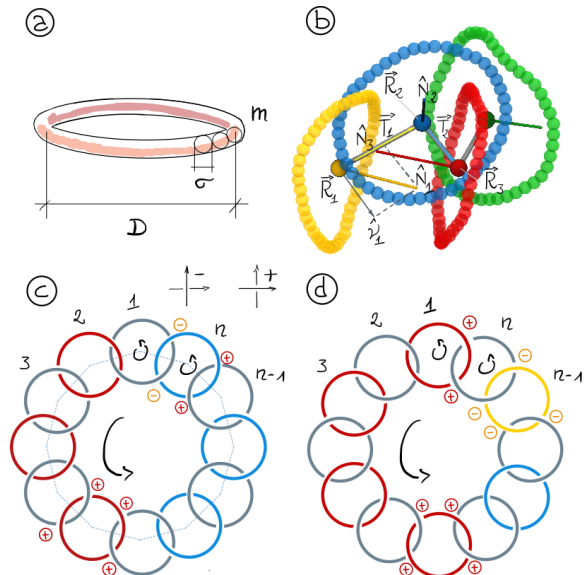


Figure 1. a) The annular polycatenanes we consider are composed of n identical, almost rigid rings of diameter D , each formed by m beads of diameter σ . b). The stiffness of the rings allows us to map them on their centers \mathbf{R}_i and normal vectors $\hat{\mathbf{N}}_i$. Notice how the vectors $\hat{\mathbf{N}}_i$ need not to be perpendicular to the backbone vectors \mathbf{T}_i . c) A polycatenane with torsion index n_{tr} can be obtained by using n_{tr} "torsion inducing" rings (red) and $n/2 - n_{tr}$ "freely-rotating" rings (blue). d) Equivalent polycatenanes with the same value of n_{tr} , like the one shown here, can be obtained by flipping and reorienting one or more rings.

The system is evolved with an underdamped Langevin dynamics integrated numerically with the LAMMPS package [33] with default values for the mass, temperature, and energy coefficients, damping time $\tau_d = 10\tau_{LJ}$ where τ_{LJ} is the characteristic simulation time, and integration time step $\Delta t = 0.0124\tau_{LJ}$, see SM. Starting from an initial condition with a fixed value of n_{tr} , the system is relaxed to equilibrium where an extensive sampling of the configurational space is performed. Here we consider polycatenanes composed of $n = \{20, 40, 60, 80, 100, 200, 300\}$ rings, with $n_{tr}/n = \{0, 0.1, 0.2, 0.3, 0.4, 0.5\}$.

In figure 2 we report some typical equilibrium configurations of circular polycatenanes for several values of n and different amount of n_{tr} : one can readily see that, for fixed n , configurations with large n_{tr} are more crumpled than those that are torsionally relaxed ($n_{tr} = 0$). Moreover, as n increases, torsionally stressed configurations start to form curled substructures reminiscent of the plectonemes in supercoiled DNA [34]. Although n is not very large, branched-like structures at very large scale can be observed too.

Note that the configurational space available in macroring models is more complex and richer than the

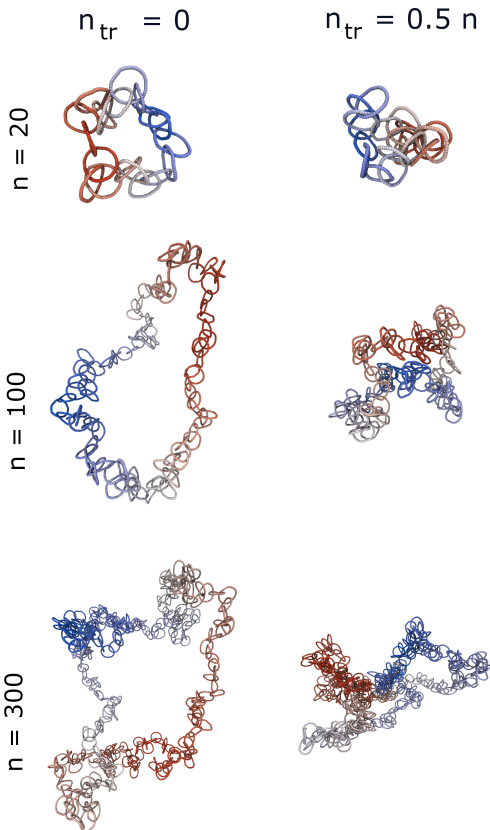


Figure 2. Typical configurations for $n = 20, 100, 300$ for two different values of n_{tr} . Left column: $n_{tr} = 0$, the polycatenanes are torsionally relaxed. Right column, $n_{tr} = 0.5n$, corresponding to the maximum torsion storable in planar circles. These last polycatenanes are visibly more compact and crumpled. The scale of the snapshot is preserved at fixed values of n . The color map highlights the sequence of the elementary rings along the backbone.

one in twistable (or ribbon-like) chain models typically used to describe dsDNA. In fact, our "monomers" are rings linearly bonded through topological constraints (Hopf links). This allows a significant degree of freedom for each ring, a local entropy, while keeping the whole system globally constrained. The consequences can be appreciated by looking at the normal-normal correlation function $C_n(d) = \langle \frac{1}{n} \sum_{i=1}^n \hat{\mathbf{N}}_i \cdot \hat{\mathbf{N}}_{i+d} \rangle$ for different values of the stored torsion, see Fig. 3 a). As expected, for the maximum value of storable torsion, $n_{tr} = n/2$, $C(d)$ decreases slowly, confirming that some twist is stored along the catenane. Interestingly, for $n_{tr} = 0$ the correlation $C(d)$ goes to zero at $d = 1$, and then regularly oscillates between relatively large, but decreasing values for $d = 2, 4, 6$ and zero for $d = 3, 5, 7$. This behaviour can be understood by observing that in this case, each ring can freely rotate around the axis joining its two neighbours. Hence, the angle between the normals of two contiguous rings may range from 0 to 180 degrees giving an average

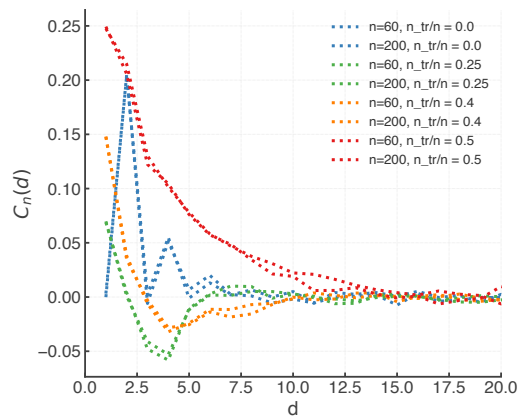


Figure 3. Normal-normal correlation function, $C_n(d)$ as a function of the index-distance d along the backbone of the polycatenane, for four different values of the fraction, $n_{tr}/n = (0, 0.25, 0.4, 0.5)$ with $n = 60$ and $n = 200$. Each ring is made by $m = 48$ beads.

of 90 degrees. This means that on average consecutive rings will lie on reciprocally orthogonal planes and that next nearest neighbours are likely to have the same orientation, i.e. $C(d) = 0$ for odd d 's and $C(d) > 0$ for even d 's (the positive sign is due to our choice of the normals in the reference configuration). Clearly, as the main direction of the backbone is changing, this peculiar even-odd behaviour tones down and disappears as d becomes sufficiently large. For $n_{tr} = \frac{n}{4}$, we see yet another set of relative orientations, with $C(d)$ reaching negative values. This remains true for $n_{tr} = 0.4n$, although the minimum is less marked. This effect appears to be due to the emergence of local conformations such as the one depicted in Fig. 1b), in which rings tend to stack together along the backbone. Such local organizations are no longer relevant when $n_{tr} = \max(n_{tr}) = n/2$. In this case the rotation of each ring around the catenane's backbone affects the position of the others.

To characterize quantitatively the effects that different amounts of locked torsional stress have on the configurational properties of the system, we coarse grain it by identifying each oriented ring i with its center of mass \mathbf{R}_i and its normal $\hat{\mathbf{N}}_i$. The resulting polygonal curve is described by the sequence of pairs of vectors $(\mathbf{R}_i, \hat{\mathbf{N}}_i)$ and bonds $\mathbf{T}_i = \mathbf{R}_{i+1} - \mathbf{R}_i$, see SM for more details. Using this coarse-grained coordinates, we computed the squared radius of gyration of the backbone for different values of n and n_{tr} : $R_g^2(n, n_{tr})$. All distances were measured in units of the ideal ring diameter, $D = \frac{m}{\pi}$. As shown in Fig. 4 a), the stored torsion affects significantly the value of $R_g^2(n, n_{tr})$: going from $n_{tr} = 0$ to $n_{tr} = \frac{n}{2}$ at fixed n the polycatenanes become roughly twice as compact. Furthermore, despite the fact that the simulated values of n are not sufficiently large to draw any conclusion on the exponent of the expected scaling behavior

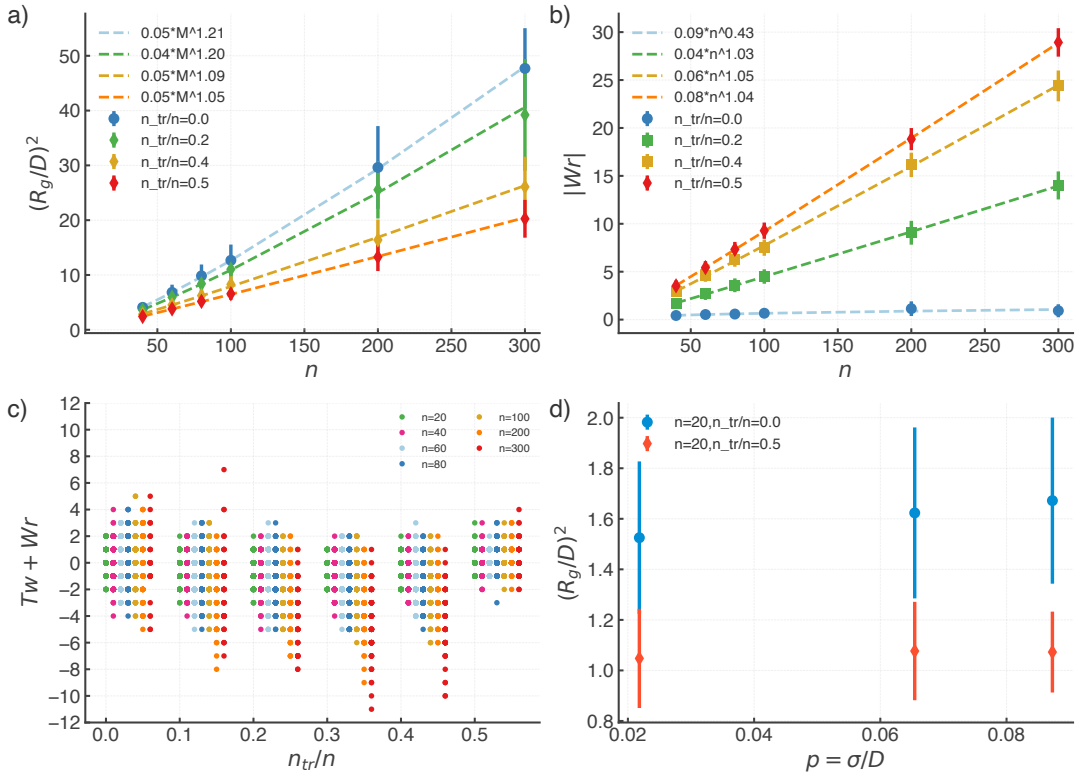


Figure 4. a) Squared radius of gyration as a function of the number of rings, n , for different values of n_{tr}/n . R_g is in units of squared diameter of an ideal ring with m beads, $D = m/\pi$. b) Scaling of the absolute value of the writhe, $|Wr|$, with n , for different values of n_{tr}/n . c) $Tw + Wr$ for different values of n_{tr}/n and n . Results for different contour length n have been shifted on the abscissa for clarity. Results for $n = 20$ include different aspect ratios p . d) Dependency of $(R_g/D)^2$ on the aspect ratio of the rings, $p = \sigma/D$, for polycatenanes with $n = 20$, having $n_{tr}/n = 0$ (upper point) and $n_{tr}/n = 0.5$ (lower points). The error bars in panles a), b), d) correspond to the standard deviation of the reported values.

$R_g^2 \sim An^{2\nu}$, the different slopes of the curves $R_g^2(n, 0)$ and $R_g^2(n, n/2)$ suggest that introducing a torsion above a certain level should at least change the amplitude A . Note that in very long dsDNA rings, the scaling behavior of the average extension crosses over to the one expected for branched polymers when supercoiling becomes relevant [34]. We expect that a similar crossover occurs also for catenanes made by a very large number of elementary rings, a condition that, however, is currently not experimentally accessible.

The fact that circular polycatenanes take on conformations which resemble a DNA with plectonemes (see also the snapshots reported in Fig. 2 for $n = 300$) can be further tested by looking at the n dependence of the absolute value of the writhe $|Wr|$, a quantity that captures the amount of coiling of a closed curve on itself [35–37]. In our case, Wr is measured on the backbone of the polycatenane, defined as the polygonal curve interpolating the centers of mass of the rings.

The behaviour of $|Wr|$ as a function of n is reported in Fig. 4 b) for different values of the stored torsion. The difference in the scaling behaviour of $|Wr|$ for relaxed and torsionally stressed polycatenanes is evident. For

the former case, $|Wr| \sim n^{1/2}$, as expected by rigorous and numerical results on unconstrained random polygons [38, 39]. On the other hand, as soon as a finite density of torsion is trapped along the circular polycatenanes, i. e. $n_{tr} > 0$, $|Wr|$ grows linearly with n with an amplitude that depends on n_{tr} . This transition from sub-linear to linear regime is a genuine effect of circular polycatenanes that cannot be observed in standard models of linear unstructured polymer chains unless they are either strongly confined [40–42] or collapsed into globular shapes by effective attractive interactions [43]

The physics of double stranded polymers as dsDNAs offers again a useful framework to characterize the conformational properties of circular polycatenanes. In the case of a dsDNA we know that circularization fixes the linking number between the two strands of the helix, Lk , via the formula $Lk = Tw + Wr$, where Tw is the total twist of the dsDNA helix around the ring backbone and the writhe Wr is the average amount of coiling of the ring on itself, as stated above [36, 37, 44]. This result is the famous Călugăreanu-White-Fuller theorem. For dsDNA, the definitions of Lk , Tw , and Wr , arise naturally from an expansion of the Gauss linking number

integral [35, 45, 46]. This is true in general for ribbon-like surfaces, if one maps the boundaries of the ribbon to two curves linked together.

In our case, the assumptions used to expand the Gauss linking number in the dsDNA case do not hold, as circular polycatenanes are not smooth; on the contrary, the local entropy of the rings can cause abrupt changes in the local properties of the macrochains. Nonetheless, since we are considering almost rigid rings, we can still define Tw as the amount of twist captured by the normals of the rings, being careful to consider only the component orthogonal to the backbone (see SM and Fig. 1b), and Wr as the total writhe of the catenane backbone. By doing this, we are implicitly mapping the macroring onto a ribbon. One of the curves defining that ribbon is provided by the coarse-grained backbone discussed earlier. The other curve connects the tips of the vectors $\hat{\nu}_k$ that are obtained by projecting the normals $\hat{\mathbf{N}}_k$ onto the direction that is perpendicular to the vectors \mathbf{t}_k forming the backbone. In this way, we can measure Tw and Wr for any circular polycatenane, and check whether and to what extent the relation $Tw + Wr = \text{constant}$ holds.

As shown in Fig. 4 c), we find that $Tw + Wr \in \mathbb{Z}$ for all configurations. As the twist angle between two consecutive normals is defined in $[-\pi, \pi]$, and our coarse-graining is equivalent to a piece-wise ribbon in which two successive normals can be twisted by an angle larger than $|\pi|$, this is equivalent to say that $Tw \bmod(1) + Wr = 0$. We verified this equivalence by taking its fractional part, and found it to hold up to a factor of order 10^{-10} , with a standard deviation of 10^{-12} , compatible with numerical round-off errors. The fact that Tw is defined $\bmod(1)$ is a known aspect of the original Călugăreanu theorem which can be dispensed away for smooth ribbon, but might be present in general [35].

Finally, we investigate how the configurational properties of the circular polycatenanes depend on the thickness-to-diameter ratio, $p = \sigma/D$, of the elementary rings. This has been done in the case of rings with $n = 20$ and $p = 0.022, 0.65$ and 0.87 .

The results, reported in Figs. 4c) and d) with $n = 20$ and twist densities $n_{tr} = 0, 10$, clearly show that $Tw \bmod(1) + Wr = 0$ regardless of the thickness of the rings, as expected. Furthermore, while the average extension of the system might depend on p in a non trivial way, as larger values of p correspond to a larger amount of twist which relaxes into writhe, we notice that, for the range of values p commonly used in self-assembled polycatenanes, the observed effective compression of the system is notable and persists over about one order of magnitude.

In conclusion, in this study we demonstrated how the circularization of properly designed polycatenanes allows the storage of a given amount of torsional stress that radically affects the equilibrium properties of these supramolecular structures, both locally and globally.

Specifically, we identify a topological parameter, n_{tr} which quantifies the amount of torsion initially stored into the polycatenane, and show that it controls both the relative orientation of nearest-neighbour rings and the scaling of R_g and $|Wr|$.

Remarkably, our results show that the Călugăreanu-White-Fuller relation holds for circular polycatenanes at least up to a factor $\bmod(1)$ in the definition of the twist: $Tw \bmod(1) + Wr = 0$ for all polycatenanes. Taken together with the result that $|Wr|$ grows as a function of n_{tr} , as shown in Fig. 4b), this suggest that it should be possible to map the polycatenane to a ribbon for which $Tw + Wr = Lk$, where Lk is an appropriate linking number. Consider for example an open, linear polycatenane with alternating links ($n_{tr} = 0$) and all normals pointing up. Clearly, one can twist its backbone by π by simply flipping the last ring or, more in general, all rings after a chosen one. If one then circularizes the polycatenane and reassigns the normals and linking numbers, the flipped ring will correspond to either a $+2$ or -2 ring, $n_{tr} = \pm 1$ (see SM for more details). Therefore, it is tempting to conclude that ± 2 rings correspond to a $\mp\pi$ twist of an equivalent ribbon and one crossing of its two boundaries. Then, if one considers the Tw given by the original normals, which would now alternate, one would get the relation $Tw + Wr = \frac{1}{2}n_{tr}$. In general though, due to the local entropy of the rings, mapping any given polycatenane configuration to an equivalent ribbon is challenging and requires further study.

Since our results remain valid for polycatenanes in good solvent conditions and over a wide range of ring thickness-to-diameter ratios, we believe they should be observable experimentally in systems ranging from DNA polycatenanes [47], synthetic polymeric polycatenanes [13, 14], to at much larger scales, macroscopic systems in which thermal fluctuations are replaced by randomized mechanical stimuli.

Finally, we believe that the model and findings presented here could be of interest for further developments in supramolecular chemistry and in the physics of soft materials, particularly soft-robotics [48, 49]. Moreover, as the Călugăreanu-White-Fuller relation links a local geometrical property, the twist, to a global one, the Writhe, our results suggest that circular chains of topologically interlocked rings could be an inspiring system for mathematicians and theoretical physicists [35, 36, 50, 51] and be exploited to build highly responsive materials with tunable properties.

The authors acknowledge the contribution of the COST Action Eutopia, CA17139. LT acknowledges support from the MIUR grant Rita Levi Montalcini. The research of FF and LT has been supported in part by the Polish National Science Centre under grant no. 2020/37/B/ST3/01471. The authors are grateful to R. Ricca and T. Tarenzi for their insight in several useful discussions.

* luca.tubiana@unitn.it

- [1] E. Orlandini and C. Micheletti, *Journal of Physics: Condensed Matter* **34**, 013002 (2021).
- [2] J. E. Lewis, M. Galli, and S. M. Goldup, *Chemical Communications* **53**, 298 (2017).
- [3] X. Liang, L. Li, J. Tang, M. Komiyama, and K. Ariga, *Bulletin of the Chemical Society of Japan* **93**, 581 (2020).
- [4] M. Kapnistos, M. Lang, D. Vlassopoulos, W. Pyckhout-Hintzen, D. Richter, D. Cho, T. Chang, and M. Rubinstein, *Nature materials* **7**, 997 (2008).
- [5] P.-G. De Gennes and P.-G. Gennes, *Scaling concepts in polymer physics* (Cornell university press, 1979).
- [6] J. Fischer, M. Lang, and J.-U. Sommer, *The Journal of chemical physics* **143**, 243114 (2015).
- [7] B. A. Krajina, A. Zhu, S. C. Heilshorn, and A. J. Spakowitz, *Physical review letters* **121**, 148001 (2018).
- [8] J. Chen, C. A. Rauch, J. H. White, P. T. Englund, and N. R. Cozzarelli, *Cell* **80**, 61 (1995).
- [9] A. R. Klotz, B. W. Soh, and P. S. Doyle, *Proceedings of the National Academy of Sciences* **117**, 121 (2020).
- [10] B. W. Soh and P. S. Doyle, *ACS Macro Letters* **9**, 944 (2020).
- [11] J. M. Polson, E. J. Garcia, and A. R. Klotz, *Soft Matter* **17**, 10505 (2021).
- [12] Q. Chen, S. C. Bae, and S. Granick, *Nature* **469**, 381 (2011).
- [13] Q. Wu, P. M. Rauscher, X. Lang, R. J. Wojtecki, J. J. De Pablo, M. J. Hore, and S. J. Rowan, *Science* **358**, 1434 (2017).
- [14] S. Datta, Y. Kato, S. Higashiharaguchi, K. Aratsu, A. Isobe, T. Saito, D. D. Prabhu, Y. Kitamoto, M. J. Hollamby, A. J. Smith, *et al.*, *Nature* **583**, 400 (2020).
- [15] M. Marendza, E. Orlandini, and C. Micheletti, *Nature communications* **9**, 1 (2018).
- [16] M. A. Ubertini and A. Rosa, *Physical Review E* **104**, 054503 (2021).
- [17] A. Livoreil, C. O. Dietrich-Buchecker, and J.-P. Sauvage, *Journal of the American Chemical Society* **116**, 9399 (1994).
- [18] L. Hu, C.-H. Lu, and I. Willner, *Nano letters* **15**, 2099 (2015).
- [19] V. Aucagne, J. Berná, J. D. Crowley, S. M. Goldup, K. D. Hänni, D. A. Leigh, P. J. Lusby, V. E. Ronaldson, A. M. Slawin, A. Viterisi, *et al.*, *Journal of the American Chemical Society* **129**, 11950 (2007).
- [20] J.-F. Ayme, J. E. Beves, C. J. Campbell, G. Gil-Ramírez, D. A. Leigh, and A. J. Stephens, *Journal of the American Chemical Society* **137**, 9812 (2015).
- [21] Y. Liu, Y. Ma, Y. Zhao, X. Sun, F. Gándara, H. Furukawa, Z. Liu, H. Zhu, C. Zhu, K. Suenaga, *et al.*, *Science* **351**, 365 (2016).
- [22] T. D. Nguyen, H.-R. Tseng, P. C. Celestre, A. H. Flood, Y. Liu, J. F. Stoddart, and J. I. Zink, *Proceedings of the National Academy of Sciences* **102**, 10029 (2005).
- [23] D. A. Leigh, J. K. Wong, F. Dehez, and F. Zerbetto, *Nature* **424**, 174 (2003).
- [24] J. V. Hernández, E. R. Kay, and D. A. Leigh, *Science* **306**, 1532 (2004).
- [25] J.-P. Sauvage, J.-P. Collin, S. Durot, J. Frey, V. Heitz, A. Sour, and C. Tock, *Comptes Rendus Chimie* **13**, 315 (2010).
- [26] S. Erbas-Cakmak, D. A. Leigh, C. T. McTernan, and A. L. Nussbaumer, *Chemical reviews* **115**, 10081 (2015).
- [27] J.-P. Sauvage, *Angewandte Chemie International Edition* **56**, 11080 (2017).
- [28] S. Mena-Hernando and E. M. Pérez, *Chemical Society Reviews* **48**, 5016 (2019).
- [29] P. M. Rauscher, S. J. Rowan, and J. J. de Pablo, *ACS Macro Letters* **7**, 938 (2018).
- [30] P. M. Rauscher, K. S. Schweizer, S. J. Rowan, and J. J. de Pablo, *The Journal of Chemical Physics* **152**, 214901 (2020).
- [31] Z. A. Dehaghani, I. Chubak, C. N. Likos, and M. R. Ejtehadi, *Soft matter* **16**, 3029 (2020).
- [32] H. Lei, J. Zhang, L. Wang, and G. Zhang, *Polymer* **212**, 123160 (2021).
- [33] S. Plimpton, *Journal of computational physics* **117**, 1 (1995).
- [34] B. A. Krajina and A. J. Spakowitz, *Biophysical journal* **111**, 1339 (2016).
- [35] H. K. Moffatt and R. L. Ricca, in *Knots And Applications* (World Scientific, 1995) pp. 251–269.
- [36] J. H. White, *American journal of mathematics* **91**, 693 (1969).
- [37] A. D. Bates, A. Maxwell, *et al.*, *DNA topology* (Oxford University Press, USA, 2005).
- [38] E. J. van Rensburg, E. Orlandini, D. Sumners, M. Tesi, and S. Whittington, *Journal of Physics A: Mathematical and General* **26**, L981 (1993).
- [39] J. Portillo, Y. Diao, R. Scharein, J. Arsuaga, and M. Vazquez, *Journal of Physics A: Mathematical and Theoretical* **44**, 275004 (2011).
- [40] E. Panagiotou, K. C. Millett, and S. Lambropoulou, *Journal of Physics A: Mathematical and Theoretical* **43**, 045208 (2010).
- [41] J. F. Marko, *Journal of statistical physics* **142**, 1353 (2011).
- [42] C. Micheletti, D. Marenduzzo, E. Orlandini, and D. Sumners, *The Journal of chemical physics* **124**, 064903 (2006).
- [43] M. Baiesi, E. Orlandini, and S. G. Whittington, *The Journal of chemical physics* **131**, 154902 (2009).
- [44] F. B. Fuller, *Proceedings of the National Academy of Sciences* **75**, 3557 (1978).
- [45] G. Calugareanu, *Rev. Math. pures appl* **4** (1959).
- [46] R. D. Kamien, *Reviews of Modern physics* **74**, 953 (2002).
- [47] T. L. Schmidt and A. Heckel, *Nano letters* **11**, 1739 (2011).
- [48] L. M. Castano and A. B. Flatau, *Smart Materials and structures* **23**, 053001 (2014).
- [49] J. Xiong, J. Chen, and P. S. Lee, *Advanced Materials* **33**, 2002640 (2021).
- [50] B. Duplantier, *Communications in mathematical physics* **82**, 41 (1981).
- [51] M. Dennis and J. Hannay, *Proceedings of the Royal Society A: Mathematical, Physical and Engineering Sciences* **461**, 3245 (2005).
- [52] K. Klenin and J. Langowski, *Biopolymers: Original Research on Biomolecules* **54**, 307 (2000).

SUPPLEMENTARY MATERIAL

Polymer model

SUPPLEMENTARY MATERIAL

Polymer model

Our polycatenanes are constituted by n elementary rings each with m beads of diameter σ . The energy associated to each configuration is given by $H = H_{intra} + H_{inter}$, where H_{intra} includes all energy terms related to a single elementary ring, and H_{inter} is the interaction energy between different elementary rings forming the polycatenane.

Specifically, for each of the n rings we define H_{intra} as follows.

$$H_{intra} = \sum_{i=1}^m \left[U_{FENE}(i, i+1) + U_{bend}(i, i+1, i+2) + \sum_{j=i+1}^m U_{WCA}(i, j) \right], \quad (1)$$

where i and j indicate the index of the bead and the modulo on m is implicitly assumed to account for the periodic nature of the rings. In the following, we use $r_{i,j}$ to indicate the norm of the vector $\mathbf{r}_i - \mathbf{r}_j$.

The FENE term, U_{FENE} is defined as follows:

$$U_{FENE}(i, i+1) = \begin{cases} -\frac{kR_0^2}{2} \ln \left[1 - \left(\frac{r_{i,i+1}}{R_0} \right)^2 \right] & \text{if } r_{i,i+1} \leq R_0 \\ 0 & \text{if } r_{i,i+1} > R_0. \end{cases} \quad (2)$$

Here the maximum extension of the bond is set to $R_0 = 1.5\sigma$ and its strength to $k = 30.0\epsilon/\sigma^2$.

The bending potential, $U_{bend}(i, i+1, i+2)$ is given by a Kratky-Porod term:

$$U_{bend}(i, i+1, i+2) = \kappa_\theta \left(1 - \frac{\mathbf{t}_i \cdot \mathbf{t}_{i+1}}{\|\mathbf{t}_i\| \|\mathbf{t}_{i+1}\|} \right), \quad (3)$$

where $\mathbf{t}_i = \mathbf{r}_{i+1} - \mathbf{r}_i$ is the i -th bond vector, $\kappa_\theta = \frac{K_B T l_p}{\sigma}$ and l_p is the persistence length. By choosing $l_p = 2m\sigma$ we consider elementary rings that are essentially rigid.

The steric interaction is accounted for by using the Weeks-Chandler-Andersen (WCA) potential:

$$U_{WCA}(i, j) = \begin{cases} 4\epsilon \left[\left(\frac{\sigma}{r_{ij}} \right)^{12} - \left(\frac{\sigma}{r_{ij}} \right)^6 \right] + \epsilon & \text{if } r_{ij} \leq 2^{1/6}\sigma \\ 0 & \text{if } r_{ij} > 2^{1/6}\sigma \end{cases} \quad (4)$$

Finally, the interaction between different rings, H_{inter}

is given by:

$$H_{inter} = \sum_{I \neq J}^n \sum_{i_I=1}^m \sum_{j_J=1}^m U_{WCA}(i_I, j_J), \quad (5)$$

where I and J run over the n elementary rings while i_I and j_J run over the beads belonging to ring I and J .

System setup

To construct an annular polycatenane with a fixed amount of quenched torsion, we proceed as follows. Given $n = 2k$ rings, we first place k of them flat on even vertices of a planar n -gon (gray rings in Fig. SI.1). Then, we complete the polycatenane by adding the rings on the odd vertices in such a way that they form either two +1 Hopf links with their neighbours (red rings in Fig. SI.1) or a -1 and +1 Hopf link (blue rings in Fig. SI.1). This is achieved by inserting suitably deformed and rotated dodecagons, as shown in Fig. SI.1. While the blue dodecagons in Fig. SI.1 can freely rotate around the axis joining the centers of their neighbours, this is not true for the red dodecagons, which cannot undergo the same rotation without affecting their neighbours. This constraint due to topology introduces a torsion to the whole polycatenane.

By varying the number n_{tr} of red rings in the interval $[0, n/2]$ we can store torsion in the system from a minimum value of 0 ($n_{tr} = 0$, torsionally relaxed polycatenane) to the maximum value $\max(n_{tr}) = n/2$. This cor-

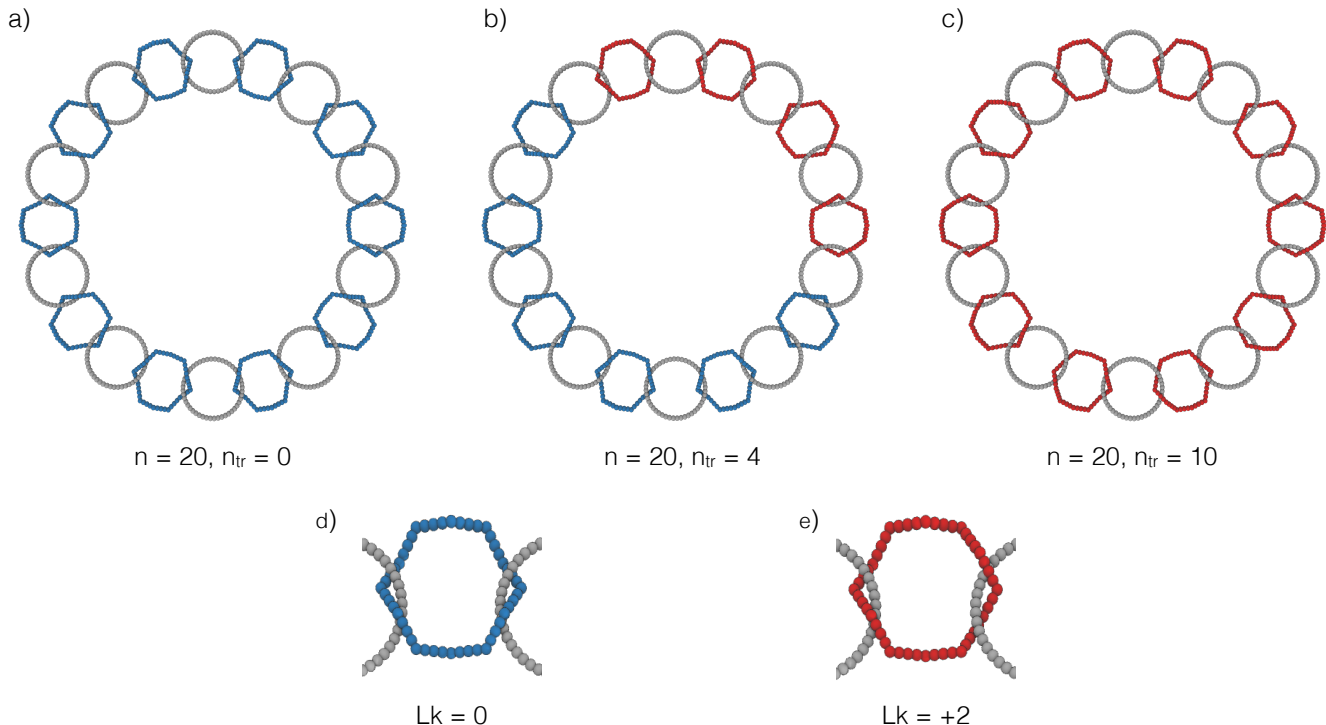


Figure SI.1. Initial configuration for (a) a zero torsion polycatenane, (b) a polycatenane with $n_{tr} = 4$ and (c) a polycatenane with $n_{tr} = 10$. Blue rings, (d), contribute a +1 and a -1 Hopf links, and thus have $Lk = 0$; red rings, (e), contribute two +1 links, $Lk = 2$.

responds to the maximum amount of twist that can be inserted into a planar circle. Higher values can be achieved by considering out-of-plane initial configurations.

To recover the desired system of semi-rigid rings, we perform an energy minimization of the system followed by a short equilibration run of the Langevin Dynamics. This is sufficient to relax the dodecagons in Fig. SI.1 into semi-rigid rings.

Equivalence of different circular polycatenanes with fixed n_{tr}

As specified above, our systems are built by inserting $n_+ = n_{tr}$ rings forming +1 Hopf links with both neighbours (+2-rings), and $n/2 - n_{tr}$ rings which do not contribute to Lk (0-rings). Note that the same amount of torsion n_{tr} can also be obtained by placing n_+ rings, each contributing to +2 Hops links (+2 rings) and n_- rings each contributing to -2 Hopf links (-2 rings), so that $n_{tr} = n_+ - n_-$. Here we show that all polycatenanes with a given value of n_{tr} have the same physical behaviour, so that the set of rings chosen to fix n_{tr} does not affect the results. To do so, we first notice that the choice of the normal of the rings is rather arbitrary, as the rings themselves do not have a physical orientation. For this reason, we can reorganize the placement of the

red, blue, and yellow rings in Fig 1 in the main text by flipping a ring with a -1 and +1 Hopf links and then re-assigning the normals so that they all point either up or down. To show that this move is sufficient to connect all polycatenanes with the same value of n_{tr} we map our system to a circular Ising chain, in which the +1 and -1 values of the spins correspond to +1 and -1 Hopf links respectively, see Fig. SI.2. Clearly, the “magnetization” of this system, $m = 2(n_+ - n_-) = 2 * n_{tr}$ corresponds to the injected torsion of the macroring. Note that the Ising chain can be seen as the dual of the circular polycatenane and the elementary rings that can be flipped without affecting their neighbours correspond to domain walls separating a +1 and a -1 spin. The flipping move on the polycatenane is then equivalent to the exchange of two spins around a wall, a move that clearly preserves the magnetization (Kawasaki move) and that can be shown to be ergodic in the space of configurations of the Ising chain with fixed m . Therefore, we can use only red (+2) and blue (0) rings to fix the value of n_{tr} in the circular polycatenane.

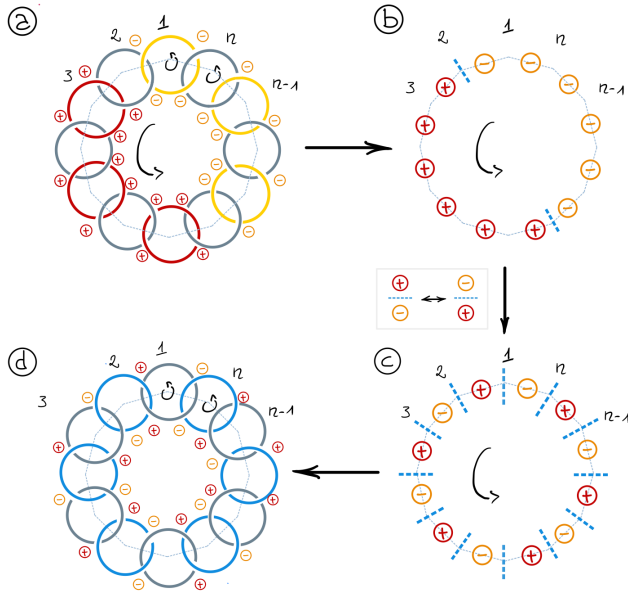


Figure SI.2. a) a polycatenane with $n_{tr} = 0$ obtained by using an equal number of +2 rings (red) and -2 rings (yellow). b) Its dual Ising lattice, where the spins correspond to the Hopf links. The system has magnetization $m = 2n_{tr}$. Rings that can be flipped without affecting their neighbours correspond to "walls" between a +1 and a -1 spin in the Ising system. c) A move which exchange both spins around a wall clearly preserve the magnetization m and is ergodic, allowing to reach conformations such as *d* in which there are no yellow rings.

Equivalence between n_{tr} and twist of a linear polycatenane

The definition of n_{tr} in our model is based on the linking number between neighboring elementary rings, which in turn depends on their orientation. One can then notice that each insertion of a +2-ring and -2 rings corresponds to a twist of the backbone of a linear polycatenane by an angle equal to $-\pi$ and $+\pi$ respectively. This is shown in Fig. SI.3.

Langevin Dynamics

The underdamped Langevin dynamics of the systems is integrated numerically using the LAMMPS package [33] with the LJ units of $\sigma = M = \epsilon = K_B = 1$, temperature $T = 1.0$ and damping time $\tau_{damp} \equiv \frac{1}{\gamma} = 10\tau_{LJ}$. Starting for a given initial configuration we evolved the system for a minimum of 10^9 steps, with timestep $\Delta t = 0.0124\tau_{LJ}$.

Conformation analyses

We characterize the equilibrium configurational properties of an annular polycatenane Γ through observables

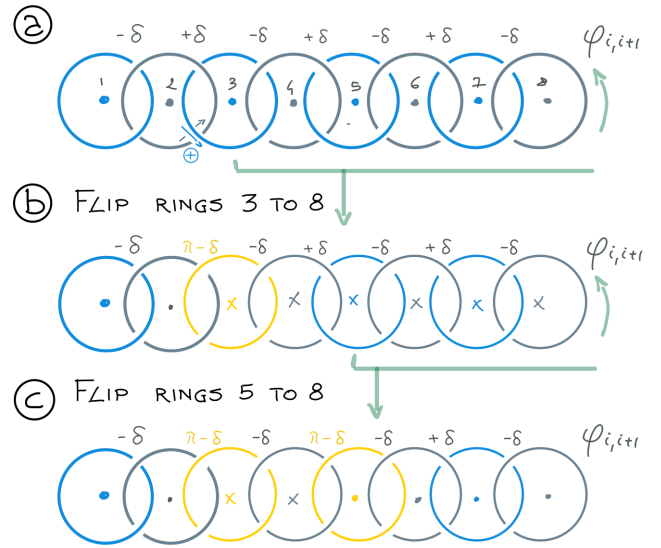


Figure SI.3. Passing from twist to ring-ring linking number. The greek letters above the polycatenanes indicate the twisting angle $\phi_{i,i+1}$ between rings i and $i+1$. Dots and crosses in the ring centers indicate normals pointing up and down respectively. The ring colors correspond to those introduced in the main text and indicate the Lk of the ring with its neighbours when all normals point up. A linear polycatenane formed by 0-rings with their normals pointing up, a), becomes a polycatenane with $n_{tr} = 2$, c), if one flips successive rings and then redefine the normals. In this simple case, each yellow ring correspond to a twist angle of $+\pi$.

such as the squared radius of gyration, $R_g^2(\Gamma)$, the Twist, $Tw(\Gamma)$, and the writhe $Wr(\Gamma)$ where $\Gamma = \{\mathbf{r}_{1,1}, \dots, \mathbf{r}_{n,m}\}$ is the set of coordinates of all beads of the elementary rings forming the polycatenane.

In order to define the twist and writhe of the polycatenane, we need to map its configuration to that of a ribbon, using the coarse-graining strategy defined below.

Coarse-graining the rings

The large persistence length of our rings guarantees that their bending fluctuations are small, keeping them almost planar. This property allows us to coarse-grain the rings by identifying them with their center of mass and their normal, as shown in Fig. SI.4. Specifically, for any index $k \in \{1, \dots, n\}$ we identify the k -esim ring with the position of its center of mass, \mathbf{R}_k , and its normal vector $\hat{\mathbf{N}}_k$. The normal vector is defined, using the indexing of the rings and following the the right-hand rule, as

$$\mathbf{N}_k = \frac{4}{m} \sum_{i=1}^{m/4} (\mathbf{r}_{i+m/4} - \mathbf{R}_k) \times (\mathbf{r}_i - \mathbf{R}_k),$$

and $\hat{\mathbf{N}}_k = \frac{\mathbf{N}_k}{|\mathbf{N}_k|}$. Note that in general an unoriented rigid ring corresponds to a dyad and not a to vector, as the

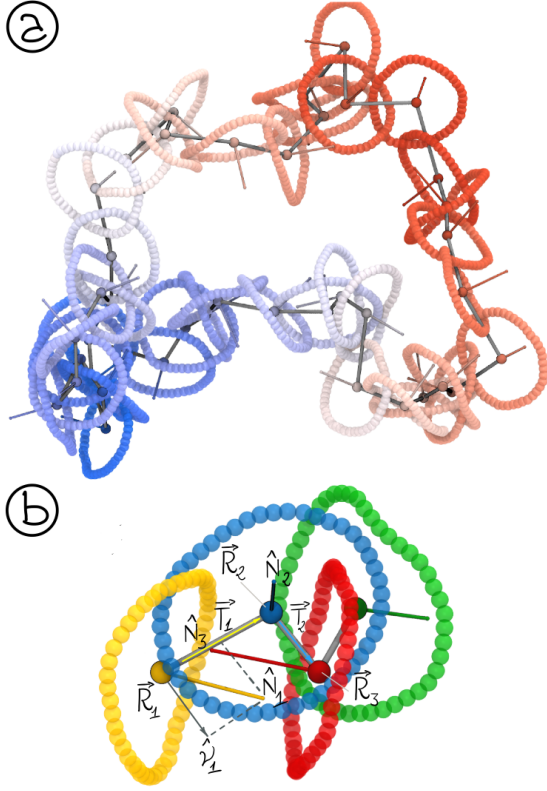


Figure SI.4. a) A conformation for a $n = 40$, $n_{tr} = 10$, $m = 48$ catenane superimposed to its coarse-grained backbone. The color map highlights the sequence of the elementary rings along the backbone. b) Coarse-grained quantities for a small set of 4 subsequent rings. For ring 1, we also show the normal to the ribbon ν_1 , obtained by subtracting from $\hat{\mathbf{N}}_1$ its projection along the bond \mathbf{T}_1 .

disc whose ring is the boundary does not have an head or tail face. The above definition of the normal versor is however possible because each elementary ring can be oriented in the reference conformation (the planar circle) as described in the main text, and this provides an ordering of the beads. Applying this coarse-graining procedure, we can thus map each the “microscopic” conformation of the polycatenane Γ into the coarse grained representation $\Gamma_{cg} = \{(\mathbf{R}_1, \hat{\mathbf{N}}_1), \dots, (\mathbf{R}_n, \hat{\mathbf{N}}_n)\}$.

Twist and writhe

By using the normal versors and the positions, \mathbf{R}_i we can define the Twist and Writhe of the coarse grained representation, following the procedure described in Klenin and Langowski in [52]. To do so, we define the tangent to the polycatenane as the bond vector joining the centers of mass of two subsequent rings: $\mathbf{T}_k = \mathbf{R}_{k+1} - \mathbf{R}_k$ for $k < n$, and $\mathbf{T}_n = \mathbf{R}_1 - \mathbf{R}_n$, where \mathbf{R}_k is the CoM of ring k . We recall that in the Călugăreanu-White-Fuller theorem the normal and tangent to the rib-

bon are orthogonal to each other at any point. Thus, we define the normal versor to the ribbon, $\hat{\nu}_k$ for the ring k as:

$$\hat{\nu}_k = \frac{\hat{\mathbf{N}}_k - (\hat{\mathbf{N}}_k \cdot \mathbf{T}_k) \mathbf{T}_k}{\|\hat{\mathbf{N}}_k - (\hat{\mathbf{N}}_k \cdot \mathbf{T}_k) \mathbf{T}_k\|}. \quad (6)$$

We define the twist of a polycatenane as:

$$Tw(\Gamma) \equiv Tw(\Gamma_{cg}) = \frac{1}{2\pi} \sum_{k=1}^n \phi_i, \quad (7)$$

with $\phi_i = \alpha_i + \gamma_i$ where α_i is the angle between $\hat{\nu}_i$ and the Frenet normal $\hat{\mathbf{B}}_i = \frac{\mathbf{T}_i \times \mathbf{T}_{i+1}}{\|\mathbf{T}_i \times \mathbf{T}_{i+1}\|}$, and γ_i is the angle between $\hat{\mathbf{B}}_i$ and $\hat{\nu}_{i+1}$. Note that ϕ_i , α_i , and γ_i are defined in the range $[-\pi, \pi]$ where the sign is determined by following the standard right-hand convention.

The writhe is defined as in [52] by summing over the solid angles $\Omega_{i,j}$ identified by bond vectors \mathbf{T}_i and \mathbf{T}_j .

$$Wr(\Gamma) \equiv Wr(\Gamma_{cg}) = \frac{1}{2\pi} \sum_{i=2}^n \sum_{j<i}^n \Omega_{ij}. \quad (8)$$

If we call 1 and 2 the starting and ending point of the tangent vector \mathbf{T}_i and 3,4 the ends of vector \mathbf{T}_j , we can define the vectors \mathbf{r}_{12} joining points 1 and 2, \mathbf{r}_{34} joining points 3 and 4, etc. Introducing the vectors

$$\begin{aligned} \mathbf{n}_1 &= \frac{\mathbf{r}_{13} \times \mathbf{r}_{14}}{\mathbf{r}_{13} \times \mathbf{r}_{14}}, & \mathbf{n}_2 &= \frac{\mathbf{r}_{14} \times \mathbf{r}_{24}}{\mathbf{r}_{14} \times \mathbf{r}_{24}}, \\ \mathbf{n}_3 &= \frac{\mathbf{r}_{24} \times \mathbf{r}_{23}}{\mathbf{r}_{24} \times \mathbf{r}_{23}}, & \mathbf{n}_4 &= \frac{\mathbf{r}_{23} \times \mathbf{r}_{13}}{\mathbf{r}_{23} \times \mathbf{r}_{13}}, \end{aligned}$$

we can finally calculate:

$$\begin{aligned} \Omega_{ij} &= \arcsin(\mathbf{n}_1 \cdot \mathbf{n}_2) + \arcsin(\mathbf{n}_2 \cdot \mathbf{n}_3) + \\ &+ \arcsin(\mathbf{n}_3 \cdot \mathbf{n}_4) + \arcsin(\mathbf{n}_4 \cdot \mathbf{n}_1). \end{aligned} \quad (9)$$

Normal-normal correlation functions

We define the normal-normal correlation function $C(d)$ as the averaged scalar product between two ring normals separated by d “bonds”:

$$C_n(d) = \left\langle \frac{1}{n} \sum_{i=1}^n \hat{\mathbf{N}}_i \cdot \hat{\mathbf{N}}_{i+d} \right\rangle_{\Gamma}, \quad (10)$$

where the average runs over the independent conformations Γ sampled by the Langevin dynamics. We note that $C_n(d)$ measures the correlation between the orientation of the normals of the elementary rings, not of the ribbon. As the rings can orient themselves with their normals almost parallel to the backbone of the polycatenane, $C_n(d)$ capture more information than the correlation between the versors $\hat{\nu}$ does